Evidence for prolate-oblate shape coexistence in the odd-A $^{73}_{35}Br_{38}$ nucleus

S. Bhattacharya,[1,2] T. Trivedi,[1,3,*] A. Mukherjee,[1] D. Negi,[4] R. P. Singh,[5] S. Muralithar,[5] S. Jehangir,[6] G. H. Bhat,[7,8] Nazira Nazir,[8] J. A. Sheikh,[8] N. Rather,[6] R. Palit,[4] S. Nag,[9] S. Rajbanshi,[10] S. Chakraborty,[11] S. Kumar,[12] M. Kumar Raju,[13] V. V. Parkar,[14] D. Choudhury,[15] R. Kumar,[5] R. K. Bhowmik,[5] S. C. Pancholi,[5] and A. K. Jain[2]

[1]*Department of Pure and Applied Physics, Guru Ghasidas Vishwavidyalaya, Bilaspur-495009, India*
[2]*Amity Institute of Nuclear Science and Technology, Amity University UP, Noida-201313, India*
[3]*Department of Physics, University of Allahabad, Allahabad-211002, India*
[4]*Department of Nuclear and Atomic Physics, Tata Institute of Fundamental Research, Mumbai-400005, India*
[5]*Inter University Accelerator Centre, New Delhi-110067, India*
[6]*Department of Physics, Islamic University of Science and Technology, Awantipora-192122, India*
[7]*Department of Physics, Sri Pratap College, Srinagar-190001, India*
[8]*Department of Physics, University of Kashmir, Srinagar-190001, India*
[9]*Department of Physics, Indian Institute of Technology (BHU), Varanasi-221005, India*
[10]*Department of Physics, Presidency University, Kolkata-700073, India*
[11]*Variable Energy Cyclotron Centre, Kolkata-700064, India*
[12]*Department of Physics and Astrophysics, University of Delhi, New Delhi-110007, India*
[13]*Department of Physics, GITAM Institute of Science, Visakhapatnam-530045, India*
[14]*Nuclear Physics Division, Bhabha Atomic Research Centre, Mumbai-400085, India*
[15]*Department of Physics, Indian Institute of Technology, Ropar-140001, India*

(Received 29 November 2021; revised 29 August 2022; accepted 27 September 2022; published 14 October 2022)

The excited states in ^{73}Br nucleus have been investigated through the fusion evaporation reaction ^{50}Cr(^{28}Si, αp)^{73}Br at a beam energy of 90 MeV using the Indian National Gamma Array. The γ-γ coincidence technique has been used to add eight new γ-ray transitions in the level scheme. The mixing ratio of $\Delta I = 0$ (mixed with $E2$ and $M1$) transitions have been determined using angular distribution and $R_{\rm DCO}$-polarization measurement. The half-life of the $9/2^+$ isomeric state has been measured to be $\tau_{1/2} = 52(2)$ ns from the variation in the intensity of delayed γ-ray transition as a function of coincidence time window. The two state mixing model calculations were performed to obtain the mixing amplitude, and mixing interaction of two different configurations of ^{73}Br. The calculated mixing amplitudes along with the deformations of two different configurations provide the monopole transition strength $\rho^2(E0)$ for Se, Br, and Kr isotopes in a semiempirical approach. These results support a prolate-oblate shape coexistence in the odd-A ^{73}Br nucleus. The observed structural properties have been discussed in terms of projected shell model calculations.

DOI: 10.1103/PhysRevC.106.044312

I. INTRODUCTION

Shape coexistence is widely spread over the nuclear chart, owing to the presence of competing "shell gaps" in the nuclear potential [1,2]. A strong interaction between the nucleons in the nuclear potential enhances the correlation energy of the system. Such interactions contribute to the origin of deformation resulting in different shapes for individual states at low excitation energy. The minima of these deformations can be vividly observed near the single particle shell gaps of the Nilsson diagram, where the minimum of the deformation energy moves towards a deformed shape in the region lying away from the shell closure. Specifically, in the $A \approx 70$ mass region, the shape driving behavior of the $g_{9/2}$ orbital results in the formation of low lying isomeric states, leading to a prolate-oblate shape coexistence [3].

In recent years, relatively light mass nuclei in the mid-shell region have attracted considerable attention due to the presence of shape coexistence in several even-even Ge, Se, and Kr isotopes [3–8]. In the ^{72}Ge nucleus, a shape isomer has been identified at the excited 0^+ state with a half-life of 444.2(8) ns [9]. Later, the multistep Coulomb excitation measurements confirm the asymmetric shape coexistence phenomena in which the prolate shaped 0^+_2 state coexists with an oblate-deformed ground state. The theoretical two state mixing model calculation also supports the presence of the prolate 0^+_2 state. In the light ^{72}Se nucleus, a shape isomer at excited 0^+_2 state having a half-life of 22.8 (14) ns was reported by Hamilton *et al.* [10]. It was suggested that the low-lying 0^+_2 state having a deformed rotational character coexists with the vibrational states associated with the spherical ground state. Afterward, the monopole transition strength around

*Corresponding author: ttrivedi1@gmail.com

31×10^3 single particle unit (SPU) obtained from the precise lifetime measurement suggests shape coexistence in this nucleus. Furthermore, Clement *et al.* reported the prolate-oblate shape coexistence in neutron deficient ^{74,76}Kr isotopes, where the ground state shows prolate character while the structure built on the 0_2^+ state corresponds to a deformed oblate shape [8]. The theoretical calculations using the beyond mean field (BMF) model-based Hartree-Fock-Bogoliubov (HFB) method [11] also support the deformed oblate character of the excited 0^+ band.

However, the abundance of shape isomer and experimental evidence confirming shape coexistence are quite limited in the odd mass nuclei lying in this region. In odd mass ^{75}Kr nucleus, Skoda *et al.* have reported the prolate-oblate shape coexistence based on the mixing ratios of $\Delta I = 0$ transitions between yrast positive parity band and excited $9/2^+$ band [12]. A similar high $K = 9/2^+$ band was also observed in ^{73}As [13]. The relativistic mean-field (RMF) calculations suggested that the positive-parity band is most likely built on the $\pi(1g_{9/2})$ configuration with a near prolate shape, while the negative parity band is characterized by the valence proton configuration $\pi(2p_{3/2}1f_{5/2}2p_{1/2})^5$ having an oblate shape. In the ^{71}Br nucleus, shape coexisting low lying states were confirmed from the half-life, 32.5(25) ns, of the shape isomeric $9/2^+$ state [14]. While in the ^{75}Br nucleus, the shape coexistence of oblate-prolate structure at the $9/2^+$ state has been predicted theoretically by using particle-rotor model and total Routhian surface calculations [15]. In our recent article on odd mass ^{73}Br [16], lying in between ^{71}Br and ^{75}Br, we have reported a prolate positive parity band along with the high $K = 9/2^+$ band. The inconsistency in the measured intensity of the excited $9/2^+$ state opens a pathway to look for the shape isomeric state leading to the conclusive evidence of shape coexistence at low spin state in this nucleus.

In the present work, we revisited our experimental data [16], and a shape isomer at the $9/2^+$ state has been determined from the measured intensity of the delayed γ ray with respect to prompt γ-ray transition. Further, seven new interconnecting transitions have been placed between the two $\Delta I = 2$ positive parity bands. The directional correlation of oriented nuclei (DCO), angular distribution from oriented nuclei (ADO), angular distribution, and linear polarization measurements were used to assign the spin and parity of these states. The mixing ratio of $\Delta I = 0$, $E2/M1$ transitions have been determined using angular distribution and $R_{\rm DCO}$-polarization measurements. The lifetime of the isomeric $9/2^+$ state has been measured from the variation of intensity as a function of coincidence time window (Δt). The two state mixing model calculations give the mixing amplitude and mixing interaction of two different configurations of ^{73}Br. Similar results obtained for other Se, Br, and Kr isotopes have been presented and compared with each other. The calculated mixing amplitude along with the deformations of two different configurations was used in the semiempirical approach to obtain monopole transition strength $\rho^2(E0)$ for Se, Br, and Kr isotopes. These semiempirical results of monopole transition strength $\rho^2(E0)$ are in reasonable agreement with the experimental monopole transition strength $\rho^2(E0)$ for even-even isotopes. These results are compared with the obtained results of the ^{73}Br nucleus to probe the shape coexistence at low excitation energy. Further, the observed band structure has been discussed in the framework of the projected shell model calculations.

II. EXPERIMENTAL DETAILS

Excited states of the ^{73}Br nucleus were populated via the ^{50}Cr(^{28}Si, αp)^{73}Br reaction at $E_{\rm lab} = 90$ MeV. The ^{28}Si beam was incident on a ^{50}Cr target of thickness 550 μg/cm^2 backed with 12 mg/cm^2 gold. The decaying γ rays were detected using the INGA array at IUAC, New Delhi [17]. A detailed description of the experimental setup is available in Refs. [16,18,19]. The RADWARE [20] and ROOT software packages [21] were used for the analysis of the γ-γ matrices. Furthermore, several γ-γ symmetric matrices with different "coincidence time windows" (viz. $\Delta t \approx$ 10, 20, 30, 40, 50, 60, 70, 80, 90, 100, 110, 120, 130, 140, 150, 160, 170, 180, 190, 200, 210, 220, and 263 ns) were constructed to manifest the lifetime of an isomeric state.

III. DATA ANALYSIS AND RESULTS

A. Level scheme

Figure 1 displays the extension of the partial level scheme of our previous study on the ^{73}Br nucleus [16] in context to the present work. The positive parity band D has been extended up to the $33/2^+$ state by placing two new 1431.2 and 1538.0 keV γ-ray transitions. In addition, four new interconnecting 1665.2, 861.2, 1821.2, and 826.7 keV γ-ray transitions have been placed between two positive parity bands A and D. The representative spectra of transition gates, 818.7 and 905.0 keV, confirming the transitions of band D are displayed in Figs. 2(a) and 2(b), respectively. Further, two new interconnecting γ-ray transitions 1366.0 and 1049.6 keV have been identified and placed between positive parity bands A and E. The representative spectrum confirming the interconnecting transitions from 583.2 and 804.0 keV transition gates are shown in Figs. 3(a) and 3(b), respectively.

The relative intensities of positive parity band D and the interconnecting transitions between bands A and E have been determined up to the $33/2^+$ state using the 187.0 keV transition gate. While the intensities of interconnecting transitions between bands A and D have been determined using 583.2, 804.0, and 994.5 keV transition gates. However, the intensity of 711.7 and 1049.6 keV transitions could not be determined due to a lack of statistics. The relative intensities of the transitions are listed in Table I. The intensity uncertainties include systematic errors, which are estimated to be 5% for 200 keV $\leqslant E_\gamma \leqslant$ 1000 keV and 10% for energies outside of this range.

B. Angular correlation and linear polarization measurements

The spin and parity of different states have been assigned based on the DCO, ADO, and linear polarization measurements. A detailed description of these measurements has already been presented in our earlier work [16,19]. In the present communication, the nature of mixed interconnecting

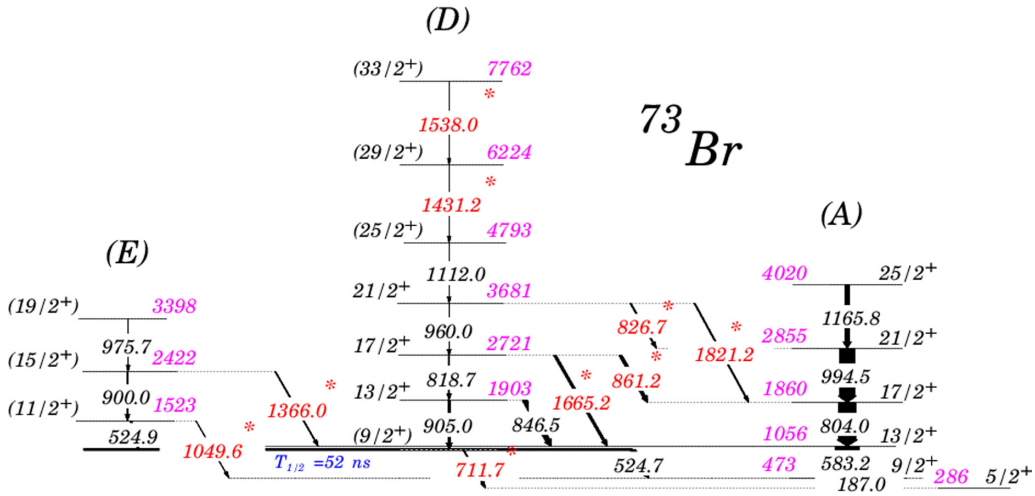

FIG. 1. Partial level scheme of ^{73}Br based on the present work and the previous study [16]. The newly observed transitions are marked by asterisks and shown in red color. All energies are in keV.

$\Delta I = 0$ transitions between bands A and D has been examined using the DCO, gated angular distribution, and linear polarization measurements.

The DCO ratios of interconnecting 524.7, 846.5, and 861.2 keV transitions between bands D and A have been determined from 905.0, 583.2, and 804.0 keV gates, respectively, as listed in Table I. The linear polarization measurement of the 861.2 keV transition has been used to assign the parity of the $17/2^+$ state at an excitation energy of 2721.3 keV. The linear polarization of the 846.5 keV transition, decaying from the $13/2^+ \rightarrow 13/2^+$ state, and 524.7 keV transition, decaying from the $(9/2^+) \rightarrow 9/2^+$ state could not be determined due to contamination arising from the target frame and due to lack of statistics, respectively. The crucial 861.2 keV transition has been assigned as $\Delta I = 0, E2/M1$ based on the $R_{\rm DCO}$ 1.18(14), linear polarization 0.49(33). The mixing ratio $+0.42^{+8}_{-15}$ of

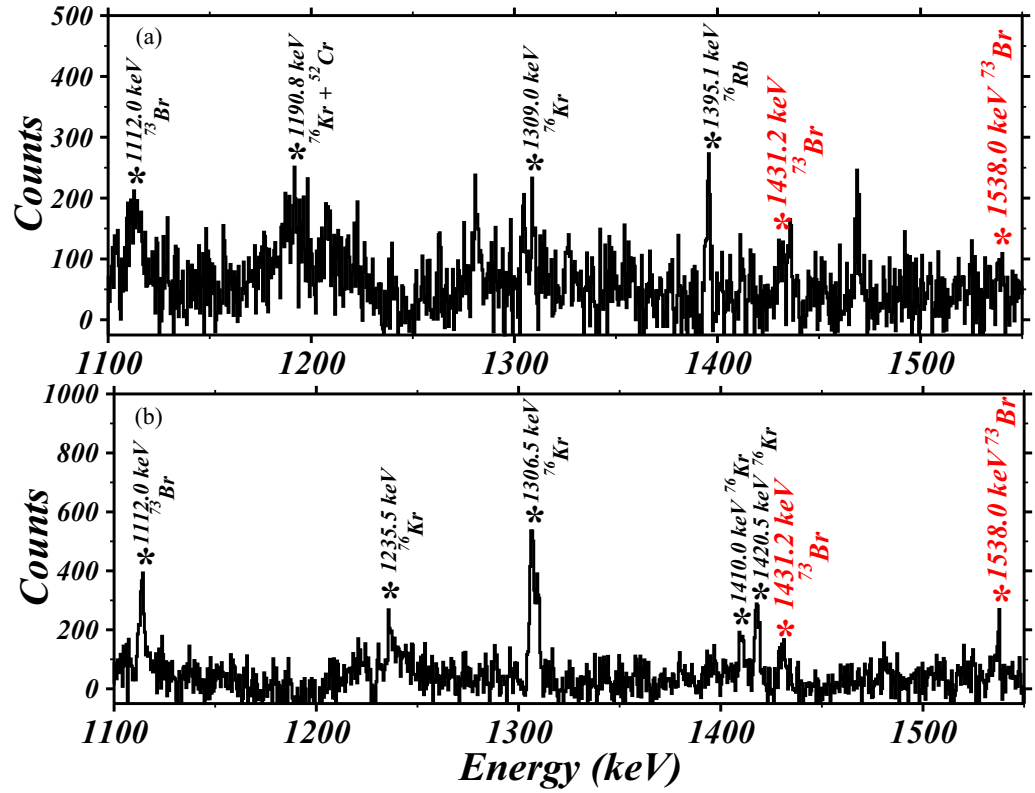

FIG. 2. A portion of the representative background subtracted spectra of 263 ns time window with the gate on (a) 818.7 and (b) 905.0 keV transitions. The newly observed transitions of ^{73}Br are labeled in red color.

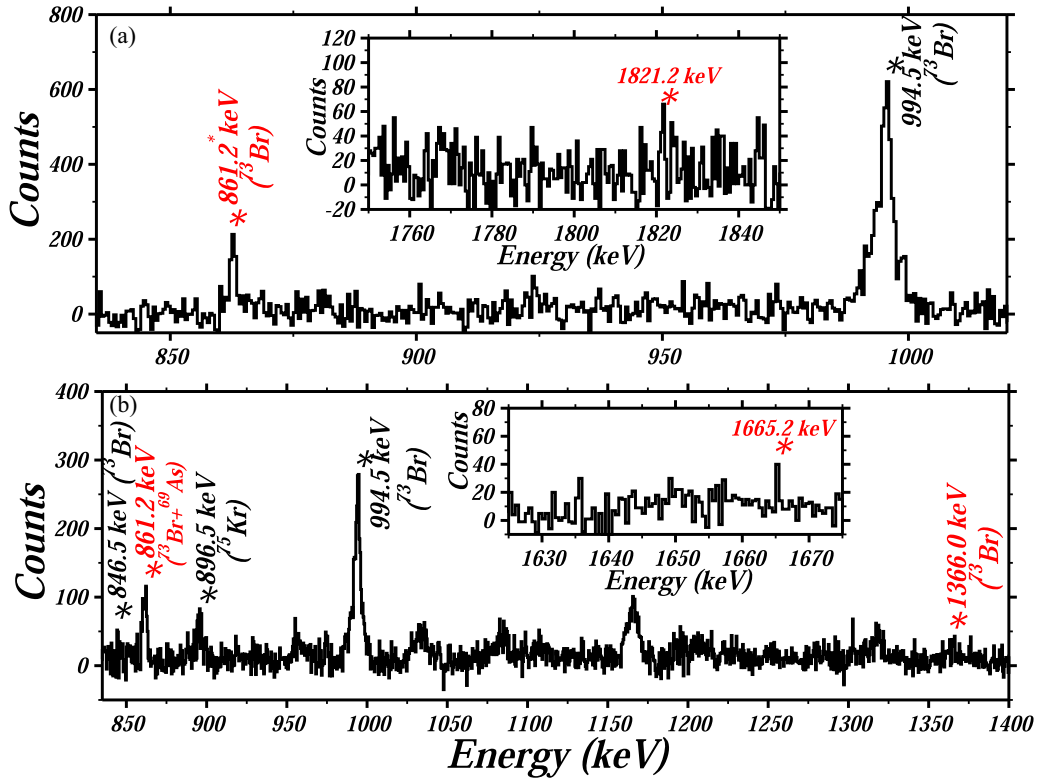

FIG. 3. Portion of the representative background subtracted spectra of 263 ns time window with the gate on (a) 804.0 and (b) 583.2 keV transitions. The newly observed transitions of ^{73}Br are labeled in red color, while insets show the newly identified 1665.2 and 1821.2 keV transitions.

TABLE I. Excitation energies (E_i), spin-parity assignments for the initial (I_i^π) and final (I_f^π) state, γ-ray transition energies (E_γ), relative intensities (I_γ), DCO ratios ($R_{\rm DCO}$), ADO ratios (R_θ), polarization asymmetry (Δ), mixing parameter from angular distribution (δ_{ad}), mixing parameter from $R_{\rm DCO}$-polarization measurement (δ_{rp}), and multipolarities assignment associated with the γ rays observed from the high-spin decay of ^{73}Br.

E_i(keV)	$(I_i^\pi) \rightarrow (I_f^\pi)$	E_γ(keV)	I_γ	$R_{\rm DCO}$	R_θ	polarization asymmetry (Δ)	δ_{ad}	δ_{rp}	Assignment
472.9	$9/2^+ \rightarrow 5/2^+$	187.0	100.0	1.07(15)	2.05(20)	—	—	—	$E2$
997.6	$9/2^{(+)} \rightarrow 9/2^+$	524.7	19.0(12)	1.17(13)	—	—	$+1.07^{+16}_{-14}$	—	$\Delta I = 0, E2/M1$
	$9/2^{(+)} \rightarrow 5/2^+$	711.7	3.5(6)	—	—	—	—	—	
1056.1	$13/2^+ \rightarrow 9/2^+$	583.2	87.6(53)	0.97(8)	2.16(11)	0.14(9)	—	—	$E2$
1522.5	$(11/2^+) \rightarrow (9/2^+)$	524.9	7.5(6)	—	—	—	—	—	—
	$(11/2^+) \rightarrow 9/2^+$	1049.6	—	—	—	—	—	—	—
1860.1	$17/2^+ \rightarrow 13/2^+$	804.0	62.1(50)	1.01(7)	1.84(9)	0.20(9)	—	—	E2
1902.6	$13/2^+ \rightarrow 9/2^+$	905.0	10.2(7)	1.40(18)	2.16(11)	0.28(17)	—	—	E2
	$13/2^+ \rightarrow 13/2^+$	846.5	16.6(11)	1.85(16)	2.42(12)	−0.20(19)	—	—	$\Delta I = 0$, E2/M1
2422.4	$(15/2^+) \rightarrow (11/2^+)$	900.0	4.4(6)	1.00(6)	1.77(11)	—	—	—	E2
	$(15/2^+) \rightarrow 13/2^+$	1366.0	0.5(2)	—	—	—	—	—	—
2721.3	$17/2^+ \rightarrow 13/2^+$	818.7	3.7(6)	1.26(19)	1.99(9)	—	—	—	E2/M1
	$17/2^+ \rightarrow 17/2^+$	861.2	10.5(7)	1.18(14)	2.25(11)	0.10(7)	$+0.62^{+13}_{-17}$	$+0.42^{+8}_{-15}$	$\Delta I = 0$, E2/M1
	$17/2^+ \rightarrow 13/2^+$	1665.2	8.5(13)	0.74(14)	1.40(17)	—	—	—	E2/M1
2854.6	$21/2^+ \rightarrow 17/2^+$	994.5	53.5(50)	1.05(10)	1.99(10)	0.19(11)	—	—	E2
3398.2	$(19/2^+) \rightarrow (15/2^+)$	975.7	0.6(6)	—	—	—	—	—	—
3681.3	$21/2^+ \rightarrow 17/2^+$	960.0	2.5(6)	—	—	—	—	—	—
	$21/2^+ \rightarrow 17/2^+$	1821.2	3.8(12)	—	—	—	—	—	—
	$21/2^+ \rightarrow 21/2^+$	826.7	3.9(12)	—	—	—	—	—	—
4020.4	$25/2^+ \rightarrow 21/2^+$	1165.8	18.1(10)	1.18(18)	1.97(20)	—	—	—	E2
4793.3	$(25/2^+) \rightarrow 21/2^+$	1112.0	<0.5	—	—	—	—		
6224.5	$(29/2^+) \rightarrow (25/2^+)$	1431.2	<0.2	—	—	—	—	—	—
7762.5	$(33/2^+) \rightarrow (29/2^+)$	1538.0	<0.2	—	—	—	—	—	—

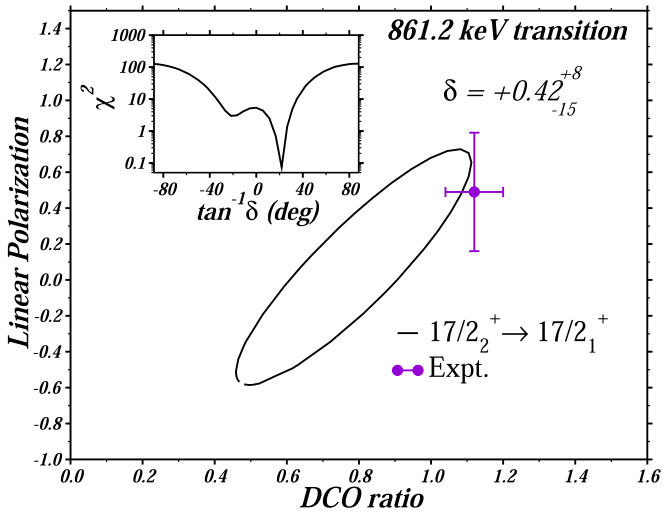

FIG. 4. The variation of R_{DCO} values as a function of linear polarization, calculated from the polarization sensitivity [19] having parameters $a = 0.532(91)$ and $b = -1.33(62) \times 10^{-4}$, for different mixing ratios (δ) of the $\Delta I = 0$, 861.2 keV transition in ^{73}Br. The violet color circle indicates the experimental data point for the 861.2-keV transition. The inset shows the χ^2 analysis for the experimental distribution of 861.2 keV transition assuming the spin sequence $17/2^+ \rightarrow 17/2^+$ with the mixing parameter $\delta = +0.42^{+8}_{-15}$.

this transition was obtained from the χ^2 minimization of experimental R_{DCO} and linear polarization using the formula mentioned in Ref. [22] as shown in Fig. 4. The uncertainty in the mixing ratio was calculated by finding the range of $\tan^{-1}\delta$ for which the $\chi^2_{\mathrm{min}} + 1$ value is reached.

To obtain clarity in the I^π assignment of the excited $9/2^+$ state of the ^{73}Br nucleus, the angular distribution of the 524.7 keV transition has been measured using a 905.0 keV transition gate. The angular distribution coefficients, $a_2 = +0.30$ and $a_4 = -0.1312$, indicate that it could be either a $\Delta I = 0$ or $\Delta I = 2$, transition. To get a conclusive assignment, a contour of a_2 and a_4 coefficients is shown in Fig. 5(a) using different spin combinations ($9/2 \rightarrow 9/2$, $11/2 \rightarrow 9/2$, and $13/2 \rightarrow 9/2$) for all possible values of δ. The comparison of the experimentally observed a_2 and a_4 coefficients with theoretical contour plot, assures the $\Delta I = 0$ assignment of the 524.7 keV transition. Further, the χ^2 minimization of the experimental attenuation coefficients gives the mixing parameter $\delta = +1.07^{+16}_{-14}$ which suggests that it has $53\%^{+10}_{-14}$ $E2$ character and the remaining $47\%^{+14}_{-10}$ $M1$ character. Similarly, the angular distribution of the 861.2 keV transition has been measured using an 804.0 keV transition gate. The angular distribution coefficients, $a_2 = +0.33$ and $a_4 = -0.07$, indicate that it could be either a $\Delta I = 0$ or $\Delta I = 2$ transition. A comparison of the experimentally observed a_2 and a_4 coefficients with theoretical contour plot assures the $\Delta I = 0$ assignment of the 861.2 transition which is shown in Fig. 5(b). The χ^2 minimization of the experimental attenuation coefficients gives the mixing parameter $\delta = +0.62^{+13}_{-17}$. Therefore, the average mixing ratio $\delta = +0.52^{+15}_{-23}$ for the 861.2 keV transition suggests that it has $21\%^{+10}_{-14}$ $E2$ character and the remaining $79\%^{+14}_{-10}$ $M1$ character.

C. Lifetime of isomeric state

The lifetime of the isomeric state has been determined from the time difference between prompt and delayed γ-ray transitions using the following empirical relation [23]:

$$N_t = N_0(1 - Ae^{\frac{-ln2\times\Delta t}{\tau_{1/2}}}), \tag{1}$$

where N_t is the population of the isomeric level at coincidence time t, N_0 is the population of the isomeric level at maximum coincidence time, Δt is the difference of coincidence time,

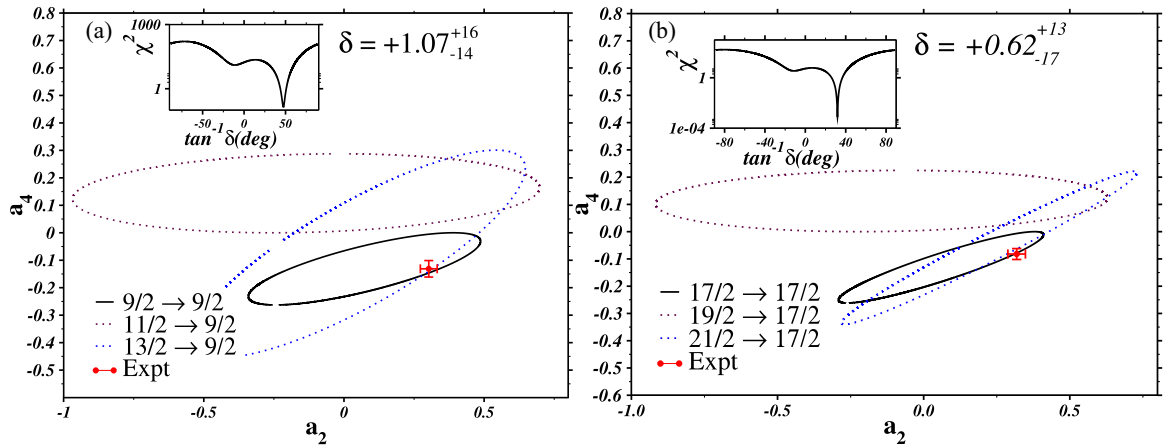

FIG. 5. (a) Angular distribution coefficients a_2 vs a_4 plot for different mixing parameters (δ) using $9/2 \rightarrow 9/2$, $11/2 \rightarrow 9/2$, and $13/2 \rightarrow 9/2$ spin sequences. The red color circle indicates the experimental data point for the 524.7 keV transition. The inset shows the χ^2 analysis for the $\Delta I = 0$, $9/2 \rightarrow 9/2$, 524.7 keV transition which gives us a $E2/M1$ transition with the mixing parameter $\delta = +1.07^{+16}_{-14}$ (b) Angular distribution coefficients a_2 vs a_4 plot for different mixing parameters (δ) using $17/2 \rightarrow 17/2$, $19/2 \rightarrow 17/2$, and $21/2 \rightarrow 17/2$ spin sequences. The red color circle indicates the experimental data point for the 861.2 keV transition. The inset shows the χ^2 analysis for the $\Delta I = 0$, $17/2 \rightarrow 17/2$, 861.2 keV transition which gives us a $E2/M1$ transition with the mixing parameter $\delta = +0.62^{+13}_{-17}$.

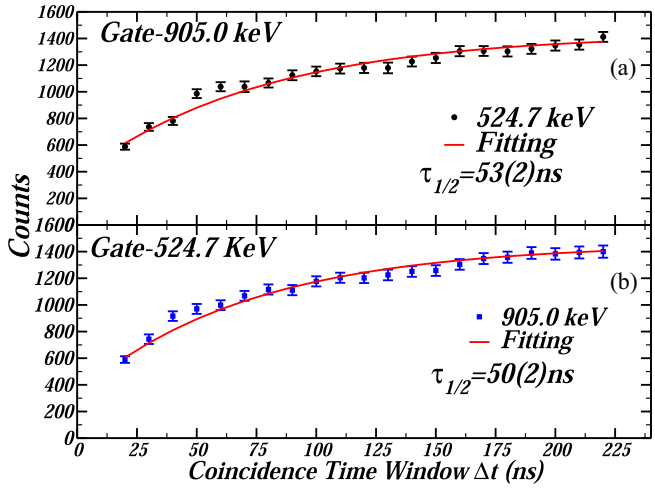

FIG. 6. (a) Variation of intensities for 524.7 keV γ-ray transitions observed from the 905.0 keV energy gate, as a function of coincidence time window. (b) Plot of intensities of 905.0 keV γ-ray transitions observed from the 524.7 keV energy gate, as a function of coincidence time window.

$\tau_{1/2}$ is the half-life of the isomeric state, and A is a fitting parameter.

In the present work, the half-life of the excited $9/2^+$ state has been determined from the variation in the intensity of the delayed γ-ray transitions as a function of coincidence time window. Figure 6(a) shows the fitting of the intensity variation of 524.7 keV transition, placed below the isomeric $9/2^+$ state, as a function of different time windows (Δt) using the 905.0 keV transition gate. The observed fitting parameter and half-life $\tau_{1/2}$ of the $9/2^+$ isomeric state is 0.76(0.06) and 53(2) ns, respectively. Further, the 905.0 keV transition, placed above the isomeric level, acts as a delayed γ-ray transition with respect to the 524.7 keV transition gate. The variation in the intensity of 905.0 keV transition is fitted as a function of the coincidence time window using the 524.7 keV transition gate as shown in Fig. 6(b). This measurement provides the half-life of the isomeric state around 50(2) ns. Thus, the average $\tau_{1/2}$ obtained for the $9/2^+$ isomeric state is 52(2) ns, which is comparable with the other shape isomers observed in this mass region [6,14]. The uncertainties quoted in the lifetimes do not include systematic error due to the experimental setup, which can be as large as 8–10%.

IV. DISCUSSION

A. Shape coexistence

One of the primary signatures of shape coexistence is the presence of a shape isomer at low excitation which often decays to the ground state via $E0$ transition indicating the mixing of shapes. In the case of even-even nuclei the decaying pure $E0$ transition, arising due to internal conversion, electron-positron pair emission (if the transition energy is above 1022 keV), or double photon emission, is only possible between spin zero and positive parity states [24]. However, for spins greater than zero the decaying $E0$ transition will compete with both $M1$ and $E2$ characters, so the total transition rate will also include the contributions from the γ decay having $M1$ and $E2$ multipolarities, as well as conversion electrons leading to $E0$, $M1$, and $E2$ admixture [24].

In the present study, the $9/2_2^+$ state, at an excitation energy of 997.6 keV, is found to be isomeric with a lifetime of 52(2) ns. The $9/2_2^+$ state decays to $9/2_1^+$ via $\Delta I = 0$, $E2/M1$ 524.7 keV transition. The mixing of $M1$ and $E2$ multipolarities in $\Delta I = 0$ 524.7 keV γ-ray transition has been measured using the gated angular distribution method as shown in Table I. The value of the mixing ratio $(\delta) = +1.07^{+16}_{-14}$ of 524.7 keV $\Delta I = 0$, $E2/M1$ transition shows that nearly $53\%^{+10}_{-14}$ $E2$ character is mixed with $47\%^{+14}_{-10}$ $M1$ character. Table II shows a comparison of the lifetime of isomeric state and mixing amplitude of $9/2_2^+$ state in ^{73}Br with the neighboring Se, Br, and Kr isotopes where shape coexistence has been established. Moreover, in the present study, several interconnecting $E2$ and $\Delta I = 0$, $E2/M1$ transitions have been placed between the two positive parity bands A and D. The mixed character of $\Delta I = 0$, $E2/M1$ 861.2 keV transition is confirmed from the DCO, linear polarization, and gated angular distribution measurements. It shows that the percentage of $E2$ fraction in 861.2 keV transition, decaying from $17/2_2^+$ to $17/2_1^+$ is $21\%^{+10}_{-14}$.

Heyde and Meyer have pointed out another interesting parameter, the size of the $E0$ matrix element which can be determined from the mixing between nuclear states with largely different radii and deformations [25]. The monopole operator connecting $J \rightarrow J$ state is described in terms of the deformation parameters β and γ as

$$m(E0) = \left(\frac{3Z}{4\pi}\right)\left[\frac{4\pi}{5} + \beta^2 + \left(\frac{5\sqrt{5}}{21\sqrt{\pi}}\right)\beta^3 \cos\gamma\right]. \quad (2)$$

This formula is based on the expression of $E0$ transition operator for a deformed uniformly charged nucleus [26]. In the limit of simple two-state mixing between configurations with deformations β_1, γ_1, β_2, and γ_2 the resulting monopole strength is given by

$$\rho^2(E0) = \left(\frac{3Z}{4\pi}\right)^2 \times a^2(1-a^2)\left[\left(\beta_1^2 - \beta_2^2\right) + \left(\frac{5\sqrt{5}}{21\sqrt{\pi}}\right) \times \left(\beta_1^3 \cos\gamma_1 - \beta_2^3 \cos\gamma_2\right)\right]^2, \quad (3)$$

where Z is the atomic number, β_1 is axial deformation of the first state, β_2 is axial deformation of the second state, γ_1 is nonaxial deformation of the first state, γ_2 is nonaxial deformation of the second state, and a^2 is the mixing amplitude of the excited state. Such mixing amplitude a^2 can be derived from the two level mixing calculations [5,27]. In this model, experimentally observed energies are considered as perturbed energies and the perturbed wave function is expressed in terms of unperturbed wave functions,

$$\psi_I = a\phi_I + b\phi_{II} \quad (4)$$

and

$$\psi_{II} = -b\phi_I + a\phi_{II}. \quad (5)$$

TABLE II. Values of lifetime, $E0$ transition energy, interaction potential (V), prolate mixing amplitude (a^2) of the excited state, experimental monopole transition strength [$\rho^2(E0)$], semiempirical (SE) results for $\rho^2(E0)$ in Se, Br, Kr isotopes [7,8,16,24,28–31].

Nuclide	$^{72}Se_{(0_2^+)}$	$^{73}Br_{(9/2_2^+)}$	$^{74}Kr_{(0_2^+)}$	$^{74}Se_{(0_2^+)}$	$^{75}Br_{(9/2_2^+)}$	$^{76}Kr_{(0_2^+)}$
Z, N	34, 38	35,38	36,38	34, 40	35,40	36,40
E_γ	937.2 keV	524.7 keV	509.0 keV	853.8 keV	627.0 keV	769.9 keV
$\tau_{1/2}$	17.5(17) ns	52(2) ns	13.0(7) ns	0.75(5) ns	—	47.3(17) ps
V	0.33	0.25	0.25	0.41	0.39	0.34
a^2	86% (1)	34% (1)	52% (1)	62%(1)	31%(1)	27%(1)
Ground state	oblate	prolate	oblate (mixed prolate)	oblate (mixed prolate)	prolate	prolate
Excited state	prolate	oblate	prolate (mixed oblate)	prolate (mixed oblate)	oblate	oblate
$\rho^2(E0)_{exp} \times 10^3$ SPU	30(5)	—	96(9)	22.9(5)	—	77(12)
$\rho^2(E0)_{SE} \times 10^3$ SPU	38(5)	55(15)	74(19)	17(10)	42(30)	90(18)

The energy of the unperturbed states can be obtained by an extrapolation of the rotational states towards lower spins. This procedure relies on the reasonable assumption that the higher spin states are not perturbed. From the energy difference of the perturbed and unperturbed states for a given spin, the mixing matrix element (V) and the mixing amplitudes (a^2) are derived in two level mixing calculations. In the present work, we have determined V and a^2 for neutron number (N) = 38 and N = 40 in Se, Br, and Kr isotopes. We noticed from Table II that the mixing amplitude (a^2) decreases when neutron number (N) or proton number (Z) increases. But the increment is more pronounced with the increasing proton numbers rather than the increasing N numbers. When N = 38, for ^{72}Se a^2 = 86% and for ^{74}Kr a^2 = 52%. When N = 40, for ^{74}Se a^2 = 62%, and for ^{76}Kr a^2 = 27%. However, when

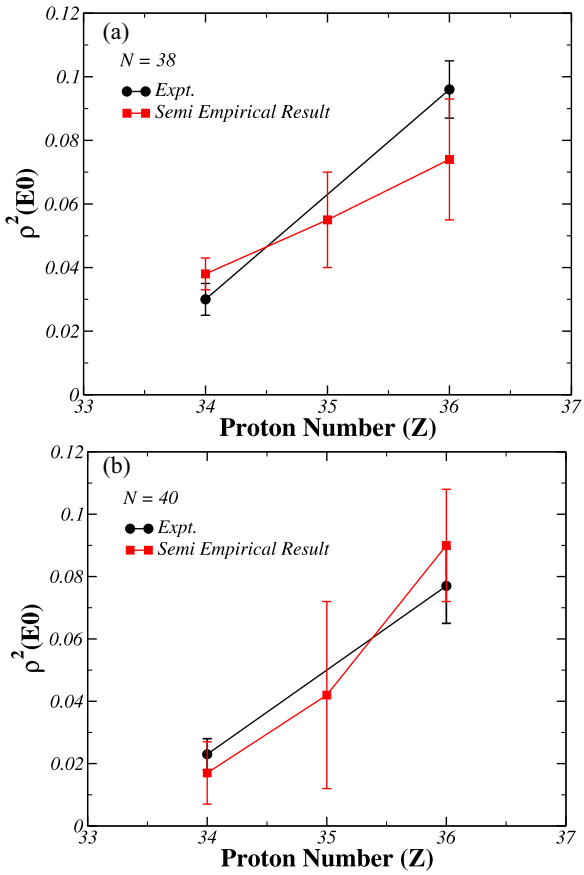

FIG. 7. Variation of monopole transition strength [$\rho^2(E0)$] as a function of proton number (Z) for (a) N = 38 isotones, (b) N = 40 in Se, Br, and Kr isotopes.

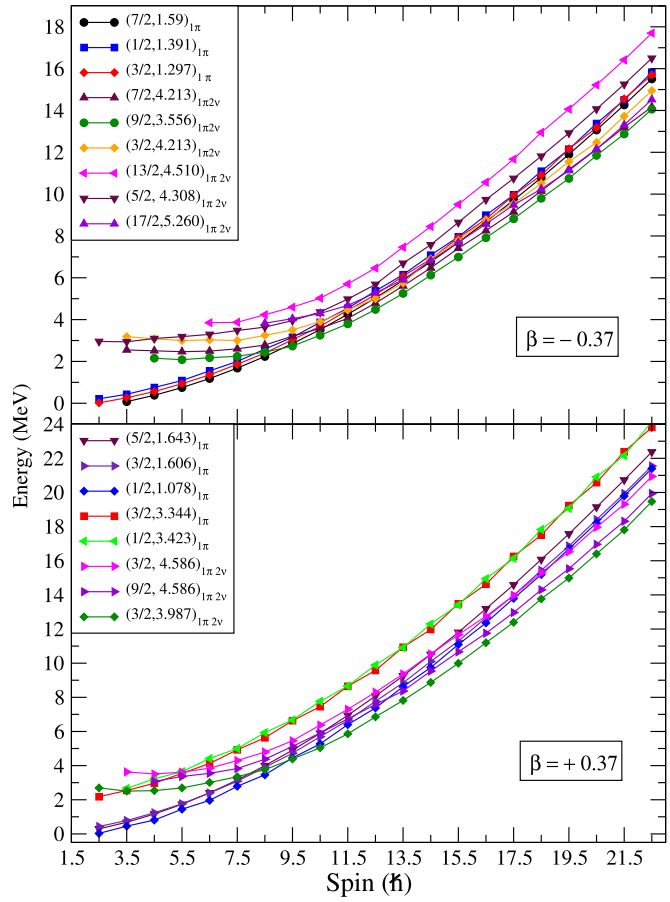

FIG. 8. Projected energies are shown before diagonalization of the shell model Hamiltonian for ^{73}Br. Only the lowest few bands are labeled by three quantities: K-quantum number, energy and group structure of the quasiparticle state. For instance, (7/2, 1.59, 1π) designates one-quasiproton state having intrinsic energy of 1.54 MeV and K = 3/2. The upper panel is with β_2 = +0.37 (prolate deformation) and lower panel is with β_2 = −0.37 (oblate deformation).

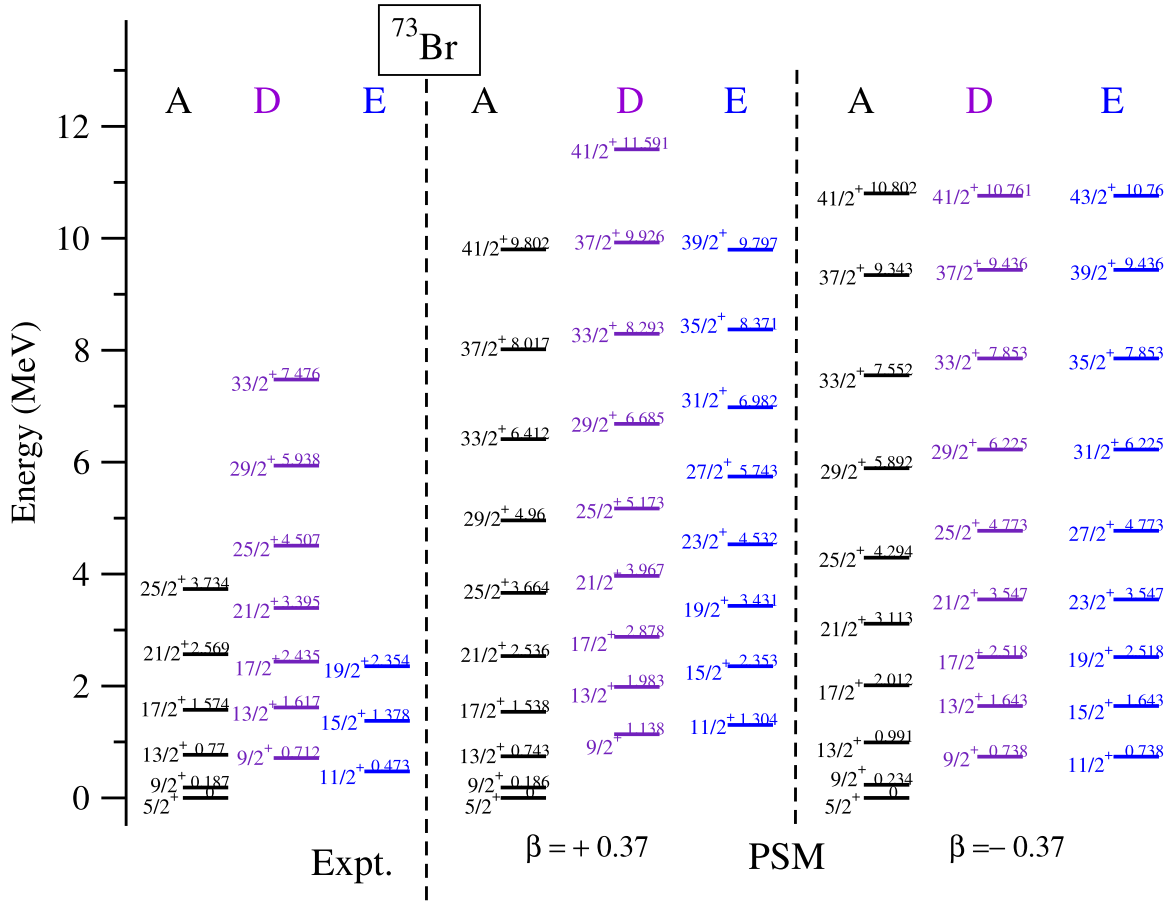

FIG. 9. The lowest PSM energies, shown for the prolate ($\beta = 0.37$) and oblate ($\beta = -0.37$) shapes, are compared with the known experimental energies. It is clarified that diagonalization (configuration mixing) is performed separately for prolate and oblate shapes using the quasiparticle basis space of Eq. 6.

$Z = 34$, for ^{72}Se $a^2 = 86\%$, and for ^{74}Se $a^2 = 62\%$. When $Z = 36$, for ^{74}Kr $a^2 = 52\%$, and for ^{76}Kr $a^2 = 27\%$. It seems that the decrement in a^2 is around ∼34–35 % for increasing Z, and ∼24-25 % for increasing N in even-even nuclei. Thus the increasing proton number puts a slightly greater influence on the decrement of mixing amplitude rather than the neutron number. In the case of odd-even nuclei the proton effectiveness is also clearly visible. The mixing amplitude (a^2) is around 34(1)% for ^{73}Br and 31(1)% for ^{75}Br. These observations show that the neutron effectiveness is very small for odd proton nuclei. Generally, the mixing amplitude (a^2) represents the component of prolate configurations in the excited state. The higher value of a^2 implies a prolate structure in the excited state. Consequently, the ground state will have an oblate structure. In general, the results obtained for the semi-empirical calculations support the experimental results for the shape of the ground state and isomeric state as shown in Table II.

Further, Kibédi *et al.* [24] have pointed out that the largest $E0$ transition strengths are consistent with changes in deformation which is a primary spectroscopic fingerprint of shape coexistence in nuclei. The variation of monopole transition strength [$\rho^2(E0)$] as a function of proton number (Z) for $N = 38$ and $N = 40$ isotones of Se, Br, and Kr isotopes are shown in Figs. 7(a) and 7(b), respectively. In the case of ^{72}Se nucleus, the experimental $\rho^2(E0) \times 10^3$ is around 30 (5) SPU which increases to 96 (9) SPU for the ^{74}Kr nucleus with the addition of two extra proton. While the experimental $\rho^2(E0) \times 10^3$ is around 22.9 (5) SPU for ^{74}Se nucleus and goes to 77 (12) SPU for ^{74}Kr nucleus with the addition of two more protons. These results also represent the proton effectiveness in monopole transition strength. The experimental monopole transition strength is not measured for odd proton ^{73,75}Br isotopes due to the limited information of experimental electron K-conversion coefficient α_K(exp) of the excited $9/2^+_2$ state. Subsequently, we have determined the semiempirical result of $\rho^2(E0)$ for $N = 38$ and $N = 40$ isotones in Se, Br, and Kr isotopes. In this calculation, we have taken the experimental deformation β_1 of the ground state [7,8,16,28–31]. While the other deformation parameters β_2, γ_1, and γ_2 are taken from the previous total Routhian surface (TRS) calculations [32,33]. The comparison of semiempirical monopole transition strength $\rho^2(E0)$ and experimental $\rho^2(E0)$ is in good agreement with each other as shown in Fig. 7. But some of the deformation β_1 taken from the previous measurements have higher uncertainty which leads to much more uncertainty

in the semiempirical result of monopole transition strength $\rho^2(E0)$.

B. Projected shell model (PSM)

In the present section, the theoretical study using the projected shell model (PSM) approach [34] is presented to substantiate the coexistence of prolate-oblate shapes for ^{73}Br nucleus in the low-spin region. The PSM model approach uses the solutions of deformed Nilsson model as the basis states. These states are then projected onto good angular-momentum states employing the projection method [35–37]. Axial symmetry is assumed in the PSM calculations, with the Nilsson states having well defined value of the projection of angular-momentum along the symmetry axis, referred to as the K quantum number. The projected basis are then used to diagonalize the shell model Hamiltonian consisting of pairing plus quadrupole-quadrupole interaction.

For the study of ^{73}Br nucleus (odd-proton system), our model space is spanned by the following angular-momentum-projected one- and three-quasiparticle (qp) basis states:

$$a_\pi^\dagger|\Phi\rangle;\ a_\pi^\dagger a_{\nu_i}^\dagger a_{\nu_j}^\dagger|\Phi\rangle; \tag{6}$$

where $|\Phi\rangle$ denote the qp vacuum $a_\nu^\dagger$ and $a_\pi^\dagger$ the qp creation operators, with the index ν (π) being the neutron (proton) quantum numbers.

As in the earlier PSM calculations, we use the quadrupole-quadrupole plus pairing Hamiltonian [34]

$$\hat{H} = \hat{H}_0 - \frac{1}{2}\chi\sum_\mu \hat{Q}_\mu^\dagger\hat{Q}_\mu - G_M\hat{P}^\dagger\hat{P} - G_Q\sum_\mu \hat{P}_\mu^\dagger\hat{P}_\mu. \tag{7}$$

Here, $\hat{H}_0$ is the spherical single-particle Hamiltonian, which contains a proper spin-orbit force [38]. The interaction strengths are taken as follows: The QQ-force strength χ is adjusted such that the physical quadrupole deformation ϵ is obtained as a result of the self-consistent mean-field HFB calculation [34]. The monopole pairing strength G_M (in MeV) is of the standard form

$$G_M = \frac{G_1 \mp G_2\frac{N-Z}{A}}{A}, \tag{8}$$

where the minus (plus) sign applies to neutrons (protons). In the present calculation, we choose G_1 and G_2 In the present calculation, we have chosen $G_1 = 20.12$ and $G_2 = 13.13$, which approximately reproduce the observed odd-even mass difference in the mass region. This choice of G_M is appropriate for the single-particle space employed in the model, where three major shells are used for each type of nucleons $N = (2, 3, 4)$ for both neutrons and protons. The quadrupole pairing strength G_Q is assumed to be proportional to G_M, and the proportionality constant being fixed as 0.16. These interaction strengths are consistent with those used earlier for the same mass region [39–41]. Finally, the quadrupole-quadrupole interaction strength χ is determined by the self-consistent relation associated with the deformation $\beta_2 = 0.37(-0.37)$ for prolate (oblate) [16]. The β_2 values are from a previous experimental measurement.

The band diagrams, which depict angular-momentum projected states for each intrinsic configuration, are shown in Fig. 8 for both prolate and oblate deformations. For the prolate shape, the ground-state band is the projected band from the intrinsic configuration of $K = 1/2$ with the quasiparticle energy of 1.08 MeV. It is also noted from the figure that the projected bands from $K = 3/2$ and $K = 5/2$ are also close to the ground-state band, and the three bands will be mixed when performing the diagonalization of the shell model Hamiltonian to obtain the final energies. For the oblate shape, on the other hand, the ground state is the projected band from $K = 7/2$ having quasiparticle energy of 1.59 MeV.

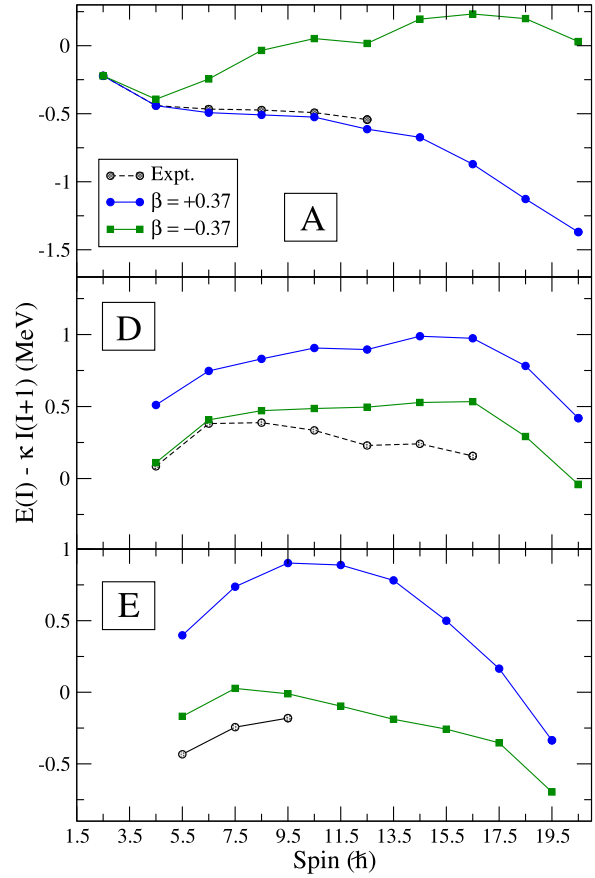

FIG. 10. PSM energies for the lowest three band after configuration mixing are plotted along with experimental data for ^{73}Br nucleus. The scaling factor κ appearing in the y axis is defined as $\kappa = 32.32A^{-5/3}$.

The projected bands depicted in Fig. 8 and many more, which are about 40 for each angular-momentum value, are used to diagonalize the shell model Hamiltonian. The lowest energies obtained for both prolate and oblate deformations are compared with the corresponding experimental energies in Fig. 9. It is evident from the figure that experimental energies are reproduced fairly well by both prolate and oblate deformation sets. In order to highlight the differences between the two shapes in comparison to the experimental data, the energies are subtracted by the core contribution, and the resulting energies are displayed in Fig. 10. It is now quite clear from this figure that band A is reproduced by considering the prolate deformation. For bands D and E, the oblate deformation appears to reproduce the experimental energies. We have also

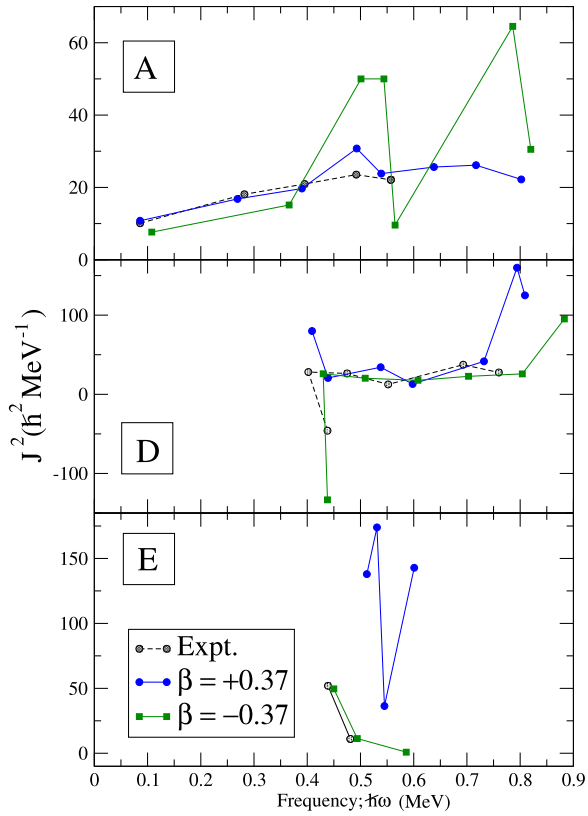

FIG. 11. Comparison of the dynamic moment of inertia, $J^{(2)} = \frac{4}{E_\gamma(I)-E_\gamma(I-2)}$. The reference band Harris parameters used are $J_0 = 23\,\hbar^2\,\mathrm{MeV}^{-1}$ and $J_1 = 90\,\hbar^4\,\mathrm{MeV}^{-3}$, obtained from the measured energy levels as well as those calculated from the PSM results, for ^{73}Br nuclei.

calculated the dynamic moment of inertia, J^2, for the three observed bands, and the results are presented in Fig. 11. It is also evident that PSM results for prolate shape agree well with the experimental numbers for band A. For bands D and E, it is J^2 calculated from the oblate shape that is in good agreement with the data.

We would like to add that the transitions observed between the oblate and prolate band structures in the experimental study cannot be calculated using the present version of the PSM approach. What is required is to use the two shapes as generator coordinates and then solve the Hill-Wheeler equation. It would then be possible to evaluate the transition between the two band structures having different shapes. In the present work, two independent sets of PSM calculations have been performed to study the band structures. We are presently working to generalize the PSM approach to perform the generator coordinate method analysis, and the results shall be presented in a future work [42].

V. SUMMARY

The excited states in the ^{73}Br nucleus have been investigated through the fusion evaporation reaction ^{50}Cr(^{28}Si, αp)^{73}Br at a beam energy of 90 MeV. The spin-parity of the states have been confirmed from the comprehensive set of spectroscopic measurements, including DCO, ADO, gated angular distribution, and linear polarization measurement. The mixing ratio of $\Delta I = 0$, $E2/M1$ transitions have been determined using angular distribution and R_{DCO}-polarization measurement. The lifetime of the isomeric $9/2^+$ state has been measured from the variation in the intensity of delayed γ-ray transition as a function of the coincidence time window. The comparison of monopole transition strength in ^{73}Br, calculated from the semiempirical approach with neighboring Se, Br, and Kr isotopes support the prolate-oblate shape coexistence at low excitation energy. Further, a comparison of experimental data with the results of PSM calculations also provides reasonable evidence for prolate-oblate shape coexistence in the odd-A ^{73}Br nucleus. In general, a stronger influence of the proton in shape coexistence is clearly visible in this mass region.

ACKNOWLEDGMENTS

The authors acknowledge the INGA collaboration for establishing the INGA array and thank the Department of Science and Technology, Government of India, for providing funds for the INGA project (Grant No. IR/S2/PF-03/2003-I). Thanks to target laboratory and pelletron staff for the smooth functioning of the accelerator. The authors would like to thank Prof. T. Kibedi for his valuable discussion on the calculation of the electronic factor. Financial support from the IUAC, New Delhi (Grant no. UFR-55313) and UGC-DAE-CSR, Kolkata (Grant no. UGC-DAE-CSR-KC/CRS/19/NP04/0915) is gratefully acknowledged. A.K.J acknowledges the support from SERB (Government of India) in the form of Grant no. CRG/2020/000770. S.R. would like to acknowledge the UGC-DAE CSR, Kolkata (Grant No. UGC-DAE-CSR/KC/CRS/19/NP13/0924) and SERB-DST for the financial support under core research grant (File No. CRG/2020/003370). The authors (G.H.B., S.J., J.A.S., N.R.) would like to acknowledge Science and Engineering Research Board (SERB), Department of Science and Technology (Government of India) for providing financial assistance under Project No. CRG/2019/004960 to carry out a part of the present research work.

[1] K. Heyde and J. L. Wood, Rev. Mod. Phys. **83**, 1467 (2011).
[2] P. E. Garrett *et al.*, Phys. Rev. Lett. **123**, 142502 (2019).
[3] A. K. Jain, B. Maheshwari, and A. Goel, *Nuclear Isomer A Primer* (Springer Nature, Switzerland, 2021), pp. 108–111.
[4] A. D. Ayangeakaa *et al.*, Phys. Lett. B **754**, 254 (2016).
[5] E. Bouchez *et al.*, Phys. Rev. Lett. **90**, 082502 (2003).
[6] C. Chandler *et al.*, Phys. Rev. C **56**, R2924 (1997).

[7] R. Palit, H. C. Jain, P. K. Joshi, J. A. Sheikh, and Y. Sun, Phys. Rev. C **63**, 024313 (2001).
[8] E. Clement *et al.*, Phys. Rev. C **75**, 054313 (2007).
[9] D. Abriola and A. A. Sonzogni, Nucl. Data Sheets **111**, 1 (2010).
[10] J. H. Hamilton *et al.*, Phys. Rev. Lett. **32**, 239 (1974).
[11] T. R. Rodríguez, Phys. Rev. C **90**, 034306 (2014).
[12] S. Skoda *et al.*, Nucl. Phys. A **633**, 565 (1998).
[13] M. K. Raju *et al.*, Phys. Rev. C **92**, 064324 (2015).
[14] S. M. Fischer, T. Anderson, P. Kerns, G. Mesoloras, D. Svelnys, C. J. Lister, D. P. Balamuth, P. A. Hausladen, and D. G. Sarantites, Phys. Rev. C **72**, 024321 (2005).
[15] G. Z. Solomon, G. D. Johns, R. A. Kaye, and S. L. Tabor, Phys. Rev. C **59**, 1339 (1999).
[16] S. Bhattacharya *et al.*, Phys. Rev. C **100**, 014315 (2019).
[17] S. Muralithar *et al.*, Nucl. Instrum. Methods Phys. Res. A **622**, 281 (2010).
[18] T. Trivedi *et al.*, Phys. Rev. C **80**, 047302 (2009).
[19] A. Mukherjee *et al.*, Phys. Rev. C **105**, 014322 (2022).
[20] D. C. Radford, Nucl. Instrum. Methods Phys. Res. A **361**, 297 (1995).
[21] R. Brun and F. Rademakers, Nucl. Instrum. Methods Phys. Res. A **389**, 81 (1997).
[22] J. R. Taylor, *An Introduction to Error Analysis: The Study of Uncertainties in Physical Measurements* (University Science Books Sausalito, California, 1997).
[23] S. Chakraborty *et al.*, Phys. Rev. C **97**, 054311 (2018).
[24] T. Kibedi, A. B. Garnsworthy, and J. L. Wood, Prog. Part. Nucl. Phys. **123**, 103930 (2022).
[25] K. Heyde and R. A. Meyer, Phys. Rev. C **37**, 2170 (1988).
[26] J. P. Davidson, Rev. Mod. Phys. **37**, 105 (1965).
[27] R. F. Casten, *Nuclear Structure from a Simple Perspective*, 2nd ed. (Oxford University Press, New York, 1990).
[28] S. L. Tabor, P. D. Cottle, J. W. Holcomb, T. D. Johnson, P. C. Womble, S. G. Buccino, and F. E. Durham, Phys. Rev. C **41**, 2658 (1990).
[29] E. A. McCutchan, C. J. Lister, T. Ahn, V. Anagnostatou, N. Cooper, M. Elvers, P. Goddard, A. Heinz, G. Ilie, D. Radeck, D. Savran, and V. Werner, Phys. Rev. C **87**, 014307 (2013).
[30] G. Mukherjee *et al.*, Nucl. Phys. A **829**, 137 (2009).
[31] https://www.nndc.bnl.gov/.
[32] P. D. Cottle *et al.*, Phys. Rev. C **42**, 1254 (1990).
[33] B. Zhi-Jun, F. Xi-Ming, J. Chang-Feng, and X. Fu-Rong, Chin. Phys. C **39**, 094101 (2015).
[34] K. Hara and Y. Sun, Int. J. Mod. Phys. E **04**, 637 (1995).
[35] P. Ring and P. Schuck, *The Nuclear Many Body Problem* (Springer-Verlag, New York, 1980).
[36] K. Hara and S. Iwasaki, Nucl. Phys. A **332**, 61 (1979).
[37] K. Hara and S. Iwasaki, Nucl. Phys. A **348**, 200 (1980).
[38] S. G. Nilsson, C. F. Tsang, A. Sobiczewski, Z. Szymanski, S. Wycech, C. Gustafson, I. Lamm, P. Moller, and B. Nilsson, Nucl. Phys. A **131**, 1 (1969).
[39] R. Palit, J. A. Sheikh, Y. Sun, and H. C. Jain, Phys. Rev. C **67**, 014321 (2003).
[40] R. Palit, J. A. Sheikh, Y. Sun, and H. C. Jain, Nucl. Phys. A **686**, 141 (2001).
[41] Y. Sun and J. A. Sheikh, Phys. Rev. C **64**, 031302(R) (2001).
[42] N. Nazir *et al.* (unpublished).